International Journal of Refrigeration 107 (2019) 191–201

Contents lists available at ScienceDirect

International Journal of Refrigeration

journal homepage: www.elsevier.com/locate/ijrefrig

Performance characterization of small variable-capacity reciprocating compressors using a minimal dataset

Guilherme Z. Santos [a], Adriano F. Ronzoni [b], Christian J.L. Hermes [a,*]

[a] POLO Labs, Department of Mechanical Engineering, Federal University of Santa Catarina, Florianópolis, SC 88040-900, Brazil
[b] Embraco Compressors, Joinville, SC 89210-035, Brazil

ARTICLE INFO

Article history:
Received 30 April 2019
Revised 19 July 2019
Accepted 20 July 2019
Available online 25 July 2019

Keywords:
Reciprocating compressor
Variable speed
Free piston
Modelling
Household refrigerator

ABSTRACT

This paper presents a semi-empirical modelling approach for predicting the performance characteristics of variable-capacity crankshaft and linear reciprocating compressors for household and light commercial refrigeration applications. The model is built on thermodynamic grounds, and its key parameters are calibrated using experimental data. A total of 33 crankshaft compressors were used for validation purposes, being 26 single-speed and 7 variable-speed, with strokes ranging from 2 to 20 cm^3. For conventional single-peed compressors, approximately 97% of the mass flow rate and 93% of the power consumption data presented errors within the 10% thresholds. For variable-speed compressors, more than 95% of the datapoints presented absolute errors lower than 10% for both power consumption and mass flow rate. In addition, the proposed approach was employed to predict the performance of a linear oil-free compressor with variable-displacement capacity control, showing errors for performance characteristics within the range of the experimental uncertainties.

Caractérisation de la performance des petits compresseurs à piston à puissance variable à l'aide d'un ensemble de données minimum

Mots-clés: Compresseur à piston; Vitesse variable; Piston libre; Modélisation; Réfrigérateur domestique

1. Introduction

Hermetic reciprocating compressors are the type most widely used for household and light commercial refrigeration appliances, in particular refrigerators and freezers. In most devices, the refrigerant is displaced by an alternating piston moved by a crank mechanism powered by an electrical motor (Tuhovcak et al., 2016), albeit linear compression technology has come onto the household refrigeration market in the past decades (Liang, 2017). In crankshaft compressors, capacity (i.e., mass flow rate) control is obtained by varying the speed of the electric motor by means of an inverter, while resonant linear compressors can modulate the stroke also allowing capacity control.

In general, roughly two-thirds of the overall energy consumed by the compressor is effectively used to compress the refrigerant, while the rest is lost due to thermodynamic, mechanical and electrical inefficiencies, being dissipated to the surrounding environment in the form of heat (Roskosch et al., 2017). The mass flow of refrigerant sucked into / discharged from the compression chamber is controlled by reed valves, whose dynamics are dependent on the differences between the in-cylinder pressure and the pressures in the suction and discharge chambers.

A schematic diagram of the compression mechanism of a positive displacement compressor is illustrated in Fig. 1. In-cylinder refrigerant compression involves four distinct processes, namely suction, compression, discharge, and expansion. Fig. 1 also illustrates all of these as the piston moves periodically from the bottom dead centre to the top dead centre, while Fig. 2 plots the thermodynamic states observed during a single compression cycle using a temperature-entropy diagram (Stouffs et al., 2001). The suction

* Corresponding author.
E-mail address: hermes@polo.ufsc.br (C.J.L. Hermes).

https://doi.org/10.1016/j.ijrefrig.2019.07.014
0140-7007/

Nomenclature

Roman

a	compression power fitting coefficients
b	mass flow rate fitting coefficients
C	compressor clearance, dimensionless
f	normalized efficiencies fitting coefficients
h	specific enthalpy, kJ kg^{-1}
k	isentropic exponent, dimensionless
$\dot{m}$	mass flow rate, kg s^{-1}
N	compressor speed, Hz
$\tilde{N}$	normalized compressor speed, dimensionless
p	pressure, Pa
$\dot{Q}$	heat transfer rate, W
q	heat released per unit mass, J kg^{-1}W
R	gas constant, J kg^{-1}K^{-1}
T	temperature, K
v	specific volume, m^3 kg^{-1}
V	volume, m^3
$\dot{W}$	compression power, W

Greek

η	Efficiency, dimensionless
$\tilde{\eta}$	Normalized efficiency, dimensionless

Subscripts

0..4	fitting coefficient indices
A..D	compression chamber volume with respect to Fig. 1
c	condensing
d	discharge
e	evaporating
id	ideal
is	isentropic
ref	reference
s	suction
sat	saturated displacement
sig	signal
sw	swept
var	variable displacement

process (DA) takes place when the in-cylinder pressure is lower than the pressure in the suction chamber, keeping the suction valve open and the refrigerant flowing. The refrigerant compression starts just after the piston has reached the bottom dead centre, increasing the in-cylinder pressure until the discharge valve opens. During the compression process, heat is exchanged between the refrigerant and the cylinder walls, producing the curve (AOB) observed in Fig. 2. At first, the refrigerant temperature (AO) is lower than the mean wall temperature and, therefore, heat is transferred from the walls to the refrigerant, increasing the entropy. After point O, the heat is then transferred from the refrigerant to the walls, reducing the flow entropy (Gosney, 1982).

The compression proceeds with the valves ideally closed until the in-cylinder pressure becomes higher than the discharge chamber pressure, opening the discharge valve and releasing the refrigerant (such a process was simplified in Fig. 1). Refrigerant is discharged until the in-cylinder and the discharge chamber pressures are equalized (BC), which occurs when the piston is at the top dead centre. From this point on, the piston starts its return, triggering the expansion process. The refrigerant expansion can be divided into two parts. In the first (CO'), the refrigerant is warmer than the cylinder walls, losing energy and decreasing its entropy. In the second (O'D), the refrigerant is colder than the walls, gaining heat and increasing its entropy. The expansion continues until the in-cylinder pressure is lower than the pressure in the suction chamber. From that point on, the compression cycle starts again.

Albeit the complexity of the reciprocating compression process, the compressor performance can be characterized by means of two key engineering parameters, namely the refrigerant mass flow rate and the compression power. Both of them depend on the geometric features, motor speed and operating conditions, such as suction and discharge pressures, and suction gas superheating. Traditionally, the compressor characteristics have been represented by polynomials fitted from experimental data according to a standardized test procedure (ASHRAE Standard S23, 1993). The polynomials usually represent the experimental data reasonably well, although they have no physical meaning and should not be used outside of the dataset range, since they perform poorly for extrapolations (Jahnig et al., 2000). Detailed physical models, such as those based on the fundamental principles (e.g., Hu et al. 2014; Prata et al., 1994), in addition to requiring prohibitive computational costs, particularly when the model is aimed at predicting the compressor performance in the refrigeration system (Diniz et al., 2018; Hermes and Melo, 2008), must be fed with parameters such as the piston-cylinder clearances, valve geometries and thermophysical properties of the oil, which is a burdensome task for the cooling system engineer interested in the performance of the refrigerator as a whole.

A third modelling strategy relies on the thermodynamics to find out the scales that rule the compression phenomena, which in turn are calibrated using experimental data. The main advantages of such an approach are the theoretical background, which allows extrapolations, and the reduced number of fitting coefficients that grants the use of smaller datasets. Different semi-empirical approaches have been proposed in the past (e.g. Cheung and Wang, 2018; Hermes and Melo, 2006; Jahnig et al., 2000; Li, 2012; Navarro et al., 2007; Negrão et al., 2011; Stouffs et al., 2001) aiming at single-speed crankshaft compressors only, albeit variable-capacity compressors have gained attention in the past decades inasmuch as nonconventional cycle architectures (Choi et al., 2018; Li, 2013; Yang et al., 2015) and advanced refrigeration controls came onto market (Oliveira et al., 2011; Piedrahita-Velásquez et al., 2014).

As a contribution to the field, this paper introduces a semi-empirical modelling approach not only for variable-speed crankshaft compressors, but also for oil-free variable-displacement linear ones relying on a minimal set of experimental datapoints for mass flow rate and power consumption. The model predictions were verified against experimental counterparts showing results within the ±10% thresholds for most cases.

2. Theoretical background

From reciprocating compressor theory (Gosney, 1982), the compression work can be defined as follows

$$\dot{W}_{id} = \dot{m} \oint v dp \tag{1}$$

Considering the indicated diagram for an ideal compressor, i.e., no reed valve pressure loss, instantaneous valve operation, and no piston-cylinder leakages, with dead volume, V_C, illustrated in Fig. 1, and assuming that the compression and expansion are isentropic processes, pv^k = constant, integration of Eq. (1) yields

$$\frac{\dot{W}_{id}}{\dot{m}} = \oint_{p_s}^{p_d} v_s (p_s/p)^{1/k} dp = p_s v_s \frac{k}{k-1}\left[\left(\frac{p_d}{p_s}\right)^{1-\frac{1}{k}} - 1\right] \tag{2}$$

Further assuming that the refrigerant behaves as an ideal gas, $pv = RT$, it follows that

$$\frac{\dot{W}_{id}}{\dot{m}} = T_s \frac{Rk}{k-1}\left[\left(\frac{p_d}{p_s}\right)^{1-\frac{1}{k}} - 1\right] \tag{3}$$

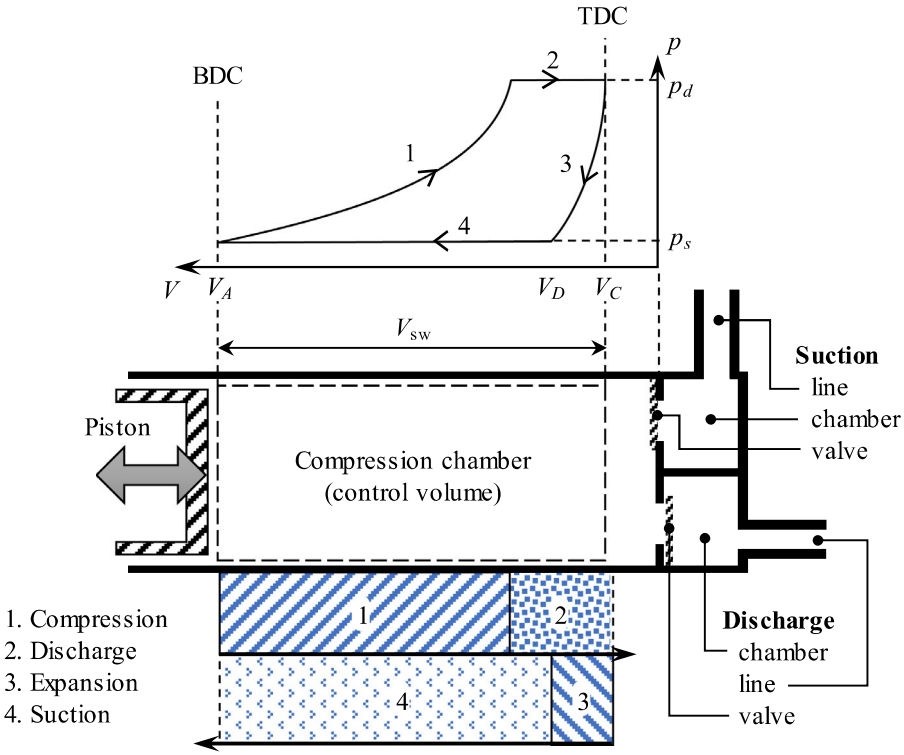

Fig. 1. Compression mechanism of a small-capacity reciprocating compressor.

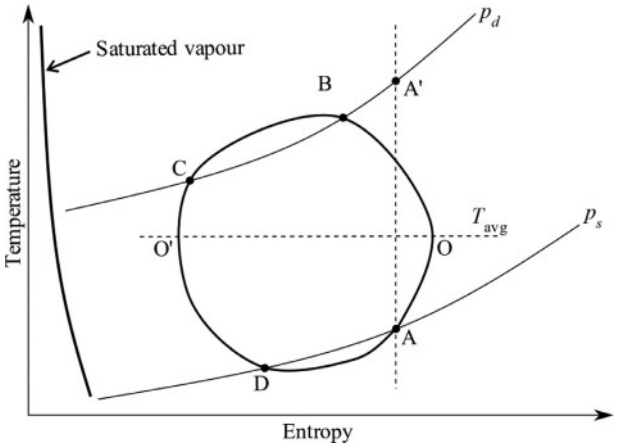

Fig. 2. Thermodynamic states observed during a compression cycle (adapted from Stouffs et al., 2001).

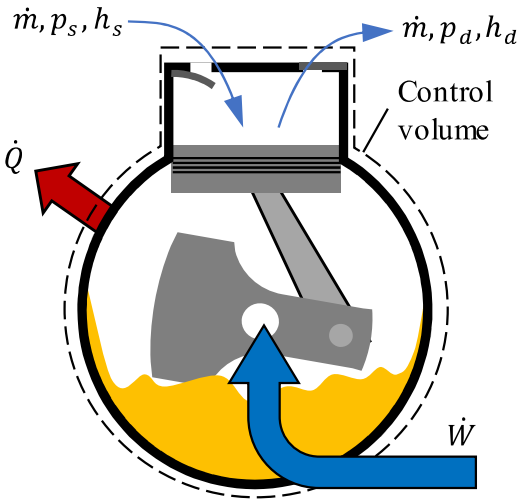

Fig. 3. Overall energy balance in a crankshaft compressor.

where T_s is the refrigerant temperature at the compressor inlet, p_s and p_d are the suction and discharge pressures, respectively, k is the isentropic exponent and R is the refrigerant gas constant.

Because of the thermodynamic irreversibilities taking place in the compression process (such as heat transfer across finite temperature difference, friction, and oil-refrigerant mixing) (Lee et al., 1982), part of the net power input to the compressor is not used for the compression, being dissipated in the form of heat and lost to the surroundings. Hence, from an overall energy balance in the control volume depicted in Fig. 3, it follows that $\dot{W} = \dot{m}(h_d - h_s) + \dot{Q}$, where the indices "s" and "d" stand for compressor suction and discharge, respectively, whereas $\dot{Q}$ is the heat transfer rate from the compressor shell to the surroundings. From the thermodynamic definition of isentropic efficiency, η_{is},

$$\eta_{is} \equiv \frac{\dot{W}_{id}}{\dot{m}(h_d - h_s)} \tag{4}$$

Therefore, the theoretical compressor power consumption, $\dot{W}$, can be calculated as follows

$$\dot{W} = \dot{m}\frac{T_s}{\eta_{is}}\frac{Rk}{k-1}\left[\left(\frac{p_d}{p_s}\right)^{1-\frac{1}{k}} - 1\right] + \dot{Q} \tag{5}$$

The mass flow rate displaced by the compressor, $\dot{m}$, is calculated from (Gosney, 1982):

$$\dot{m} = \frac{V_{sw}N}{v_s}\eta_v \tag{6}$$

where v_s is the specific volume at compressor suction, N is the compressor speed in [Hz], η_v the volumetric efficiency, and $V_{sw} = V_A - V_C$ is the swept volume, depicted in Fig. 1. From the definition of volumetric efficiency,

$$\eta_v \equiv \frac{V_A - V_D}{V_{sw}} \tag{7}$$

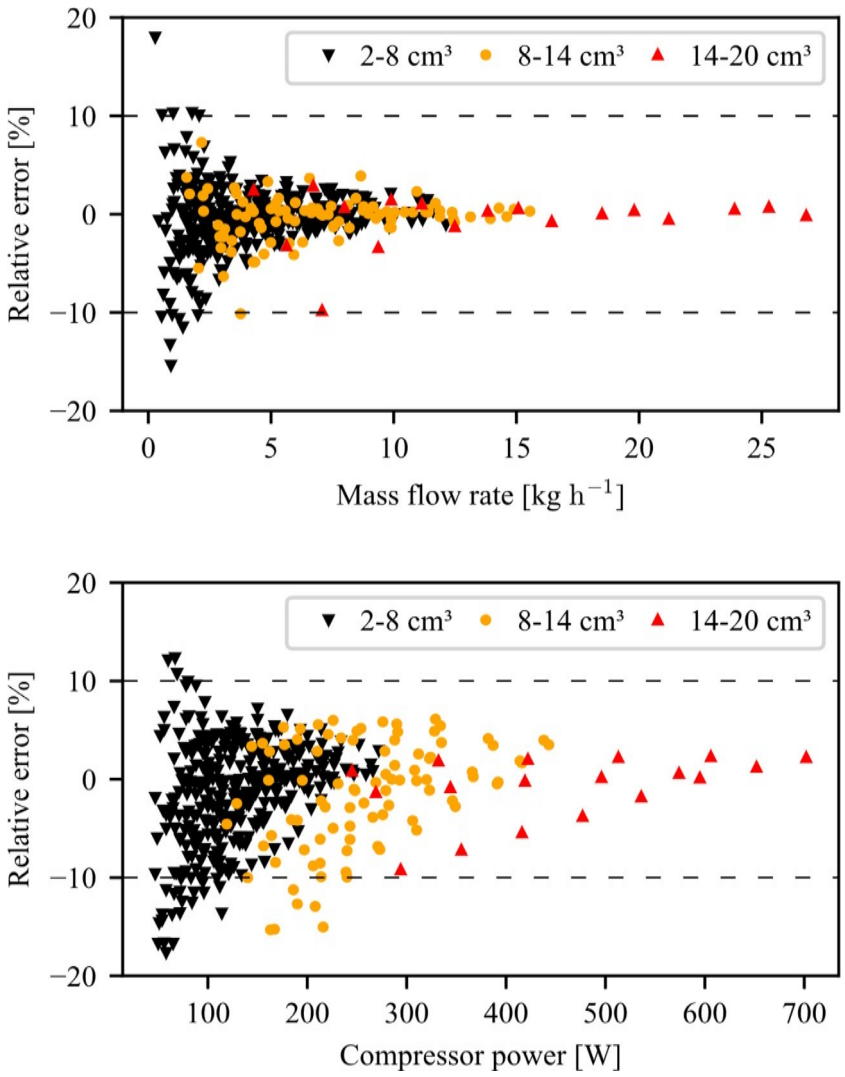

Fig. 4. Relative error of mass flow rate and compressor power for single-speed crankshaft compressors.

Thus invoking once again the assumption of isentropic compression and expansion, it follows that $V_D = CV_{sw}(p_d/p_s)^{1/k}$, where $C \equiv V_C/V_{sw}$ is the compressor clearance, resulting in $V_A = V_{sw} + V_C = V_{sw}(1 + C)$. Assuming ideal gas behavior, the theoretical mass flow rate displaced by the compressor can be expressed as follows

$$\dot{m} = \frac{p_s V_{sw} N}{RT_s}\left\{1 - C\left[\left(\frac{p_d}{p_s}\right)^{\frac{1}{k}} - 1\right]\right\} \tag{8}$$

Eqs. (5) and (8) provide the thermodynamic scales that rule the compression process, thus affecting the compressor characteristics, i.e., power consumption and mass flow rate. Semi-empirical models, based on Eqs. (5) and (8), have been widely used to describe the performance of positive-displacement compressors in the literature (e.g., Haberschill et al., 1994; Mackensen et al., 2002; Popovic and Shapiro, 1995).

More recently, an accurate model for single-speed crankshaft compressors was proposed by Li (2012) based on the classic compressor theory (Gosney, 1982) and the work of Negrão et al. (2011), consisting mostly of fitting curves for the volumetric and isentropic efficiencies as functions of the working pressures. On one hand, the mass flow rate is obtained from Eq. (6), with the volumetric efficiency calculated from

$$\eta_v = b_0 + b_1\left[\frac{p_d}{p_s(1 - b_2)}\right]^{\frac{1}{k}} \tag{9}$$

where $b_{0,1}$ are associated with the compressor clearance and b_2 represents the discharge valve pressure drop. On the other hand, the compressor power is calculated from an expression similar to Eq. (5), where the isentropic efficiency is calculated from $1/\eta_{is} = a_0 + a_1/p_d + a_2/p_s$ and $\dot{Q}$ is quantified as a fixed heat loss, independent of the mass flow rate

Later, Li (2013) extended the formulation for variable speed compressors, adopting the following expression for the compression power:

$$\dot{W} = \dot{m} p_s v_s a_0\left[\left(\frac{p_d}{p_s}\right)^{a_1 + \frac{k-1}{k}} + \frac{a_2}{p_d}\right] + a_3 \tag{10}$$

where a_0 can be associated with the isentropic efficiency and specific heat ratio (k) straightforwardly by comparing Eq. (10) with Eq. (5).

To consider the influence of the speed on the volumetric and isentropic efficiencies, quadratic polynomial expressions were used, introducing six more fitting coefficients into Li's (2013) model,

$$\tilde{\eta}_j = f_{j,1} + f_{j,2}\tilde{N} + f_{j,3}\tilde{N}^2 \tag{11}$$

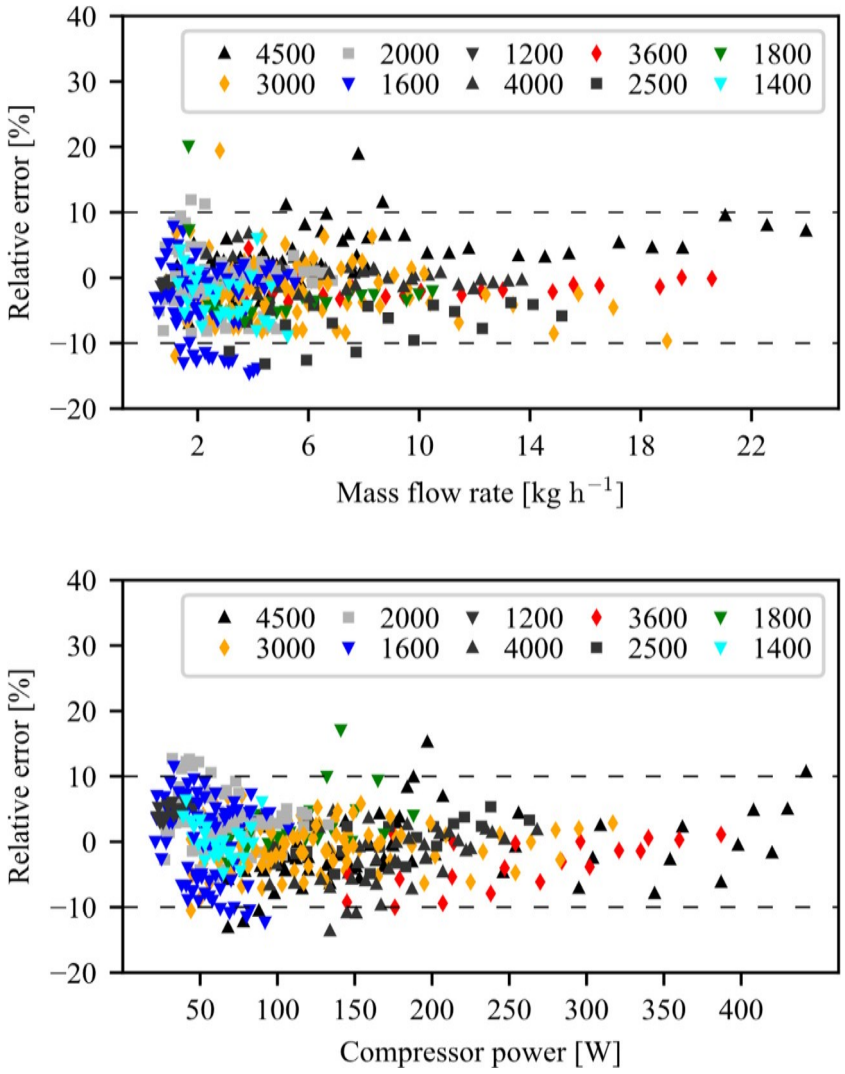

Fig. 5. Relative error of mass flow rate and compressor power for variable-speed crankshaft compressors for each compressor speed in rpm.

where j stands for either 'v' or 'is', f_j are the fitting coefficients, $\tilde{\eta} = \eta/\eta_{\text{ref}}$ is a normalized efficiency, $\tilde{N} = N/N_{\text{ref}}$ is a normalized compressor speed, and η_{ref} is the reference efficiency taken at the reference speed. Therefore, the mass flow rate at any speed can be calculated straightforwardly from Eq. (6), whereas the power consumption is obtained from $\dot{W} = \dot{W}_{\text{ref}}\tilde{N}\tilde{\eta}_v/\tilde{\eta}_{\text{is}}$. In order to reduce the number of fitting coefficients, Li (2013) came out with the following constraints, $1 = f_{j,1} + f_{j,2} + f_{j,3}$, thus decreasing the number of additional coefficients to two for each physical entity (i.e., mass flow and power consumption). At all, five coefficients are required for the mass flow rate calculations, whereas six coefficients are required for the compression power.

3. Proposed formulation

Comparing Li's model (Eqs. (9)–(11)) with the theoretical formulation (Eqs. (5) and (8)) makes clear that the former carries many coefficients that have empirical nature, some of them in meaningless mathematical functions (see, for instance, the coefficients f_j in Eq. (11)), which not only undermines the model reliability and robustness, but also increases the minimal size of the dataset required to fit the surface. A better approach would keep model background on thermodynamic grounds, so that all the fitting coefficients have physical meaning.

Thus taking Eq. (5) and assuming that the heat rejected by the compressor is proportional to the mass flow rate, it follows that $\dot{Q} = \dot{m}q$, where q is the heat per unit mass dissipated by the compressor [J kg^{-1}]. Hence, the overall compressor power consumption can be expressed as follows:

$$\dot{W} = \dot{m}\left\{\frac{T_s}{\eta_{\text{is}}}\frac{Rk}{k-1}\left[\left(\frac{p_{\text{d}}}{p_{\text{s}}}\right)^{1-\frac{1}{k}} - 1\right] + q\right\} \tag{12}$$

It is worth of note that in the formulation introduced by Negrão et al. (2011), also adopted by Li (2012, 2013) as the backbone of his correlation, the term q in Eq. (12) is replaced by w_u – the so-called specific work of the compressor unloaded – as Negrão et al. (2011) assumed that the total specific work is comprised of two terms, namely unloaded work and flow work, which in turn is the amount of specific enthalpy delivered by the compressor to the refrigerant. The first-principles formulation introduced here proves that the "unloaded work" introduced by Negrão et al. (2011) is actually the specific amount of heat dissipated by the compressor due to its irreversible losses.

The approach proposed here assumes that R, k, q and η_{is} are fairly constant in Eq. (12), in a way that such parameters can be replaced by fitting coefficients, $a_{0..2}$, yielding the following

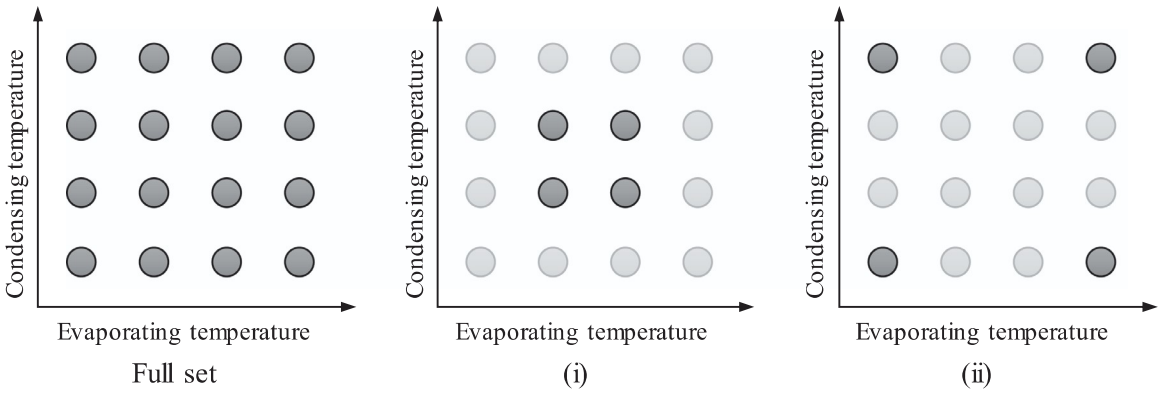

Fig. 6. Schematic representation of the datasets used for the extrapolation and experiment minimization exercises.

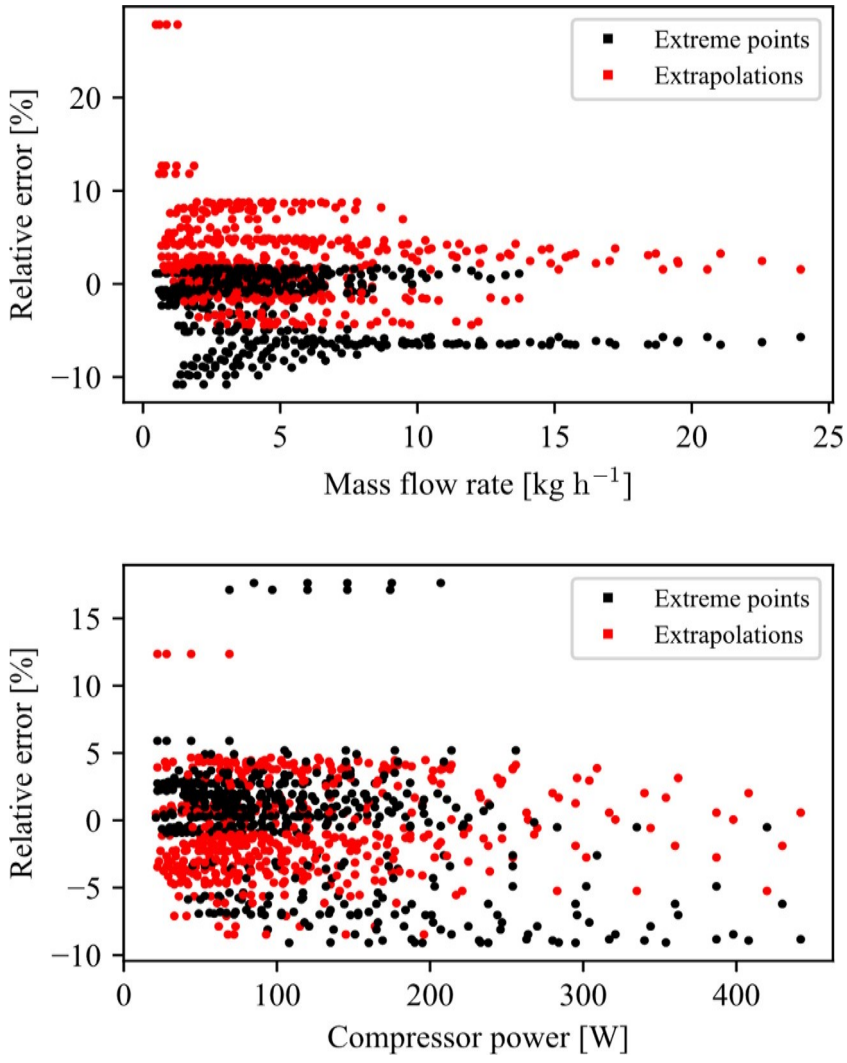

Fig. 7. Deviations of predictions using coefficients according to cases (i) and (ii) with respect to the full dataset.

expression for the overall compression power:

$$\dot{W} = \dot{m}\left\{a_0 T_s\left[\left(\frac{p_d}{p_s}\right)^{a_1} - 1\right] + a_2\right\} \tag{13}$$

where the coefficients $a_{0..2}$ are to be determined based on compressor data. It is worth noting that the refrigerant enthalpy at the compression discharge can be calculated straightforwardly from $h_d = h_s + \dot{W}/\dot{m} - a_2$, as one must discount the heat released by the compressor, embedded in a_2 in this proposed formulation, to calculate the specific work delivered to the fluid flow in the form of enthalpy. It is worth noting that Eq. (13) preserves the physical scales of the theoretical model, Eq. (12), whereas Li's (2012, 2013) correlations come out with empirical terms, such as a_2 and a_3 in Eq. (10), and f_j's in Eq. (11).

Similarly, taking Eq. (8) and noting that C, R, k and V_{sw} are fairly constant, such parameters can be replaced by fitting

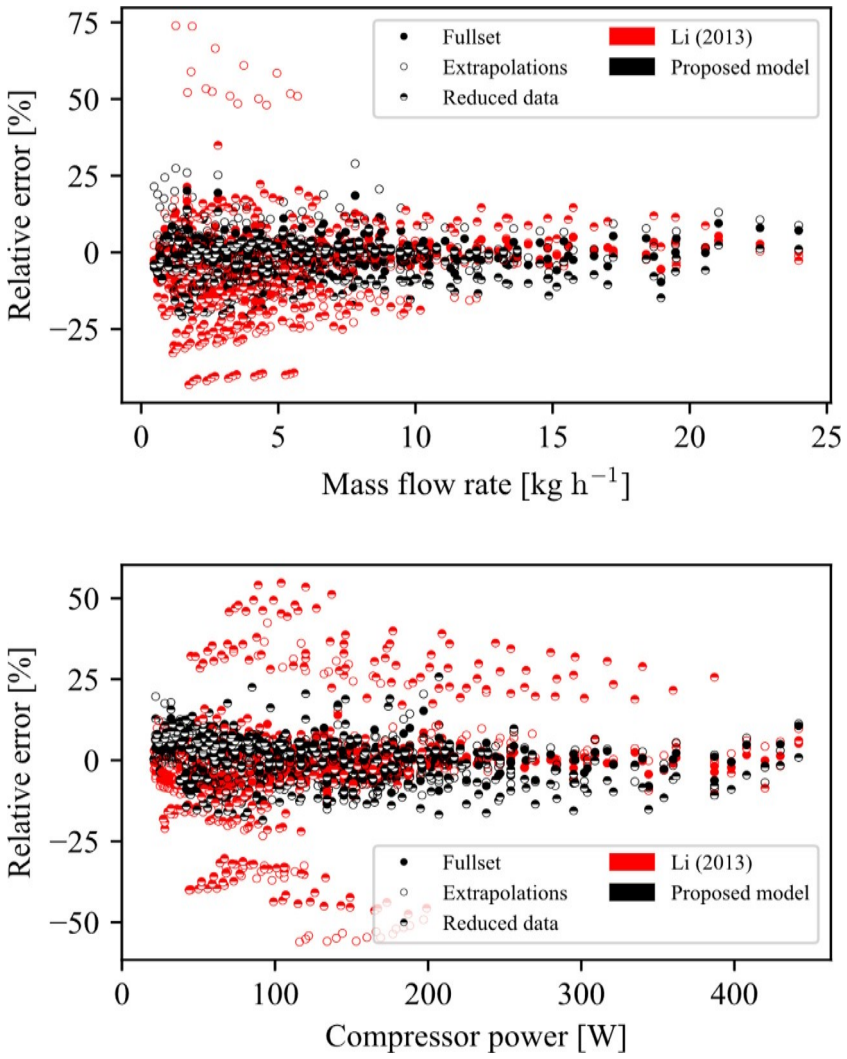

Fig. 8. Comparisons between the results from the proposed model and Li's (2013) model using different datasets.

coefficients, $b_{0..2}$, yielding the following expression for the mass flow rate:

$$\dot{m} = \frac{p_s N}{T_s}\left\{b_0 - b_1\left[\left(\frac{p_d}{p_s}\right)^{b_2} - 1\right]\right\} \tag{14}$$

where the coefficients $b_{0..2}$ are to be determined based on compressor catalogue data. Comparing Eq. (14) with the theoretical model, Eq. (8), one can see that the physical scales have been preserved, which is not the case for the Li's (2012, 2013) correlation that, in addition to the f_j coefficients in Eq. (11), also dropped the term −1, introducing a non-physical scale that might lead to poor predictions, particularly for refrigerants working with relatively low pressure ratios (e.g., R600a). It should be noted that, at all, the proposed formulation relies on three fitting coefficients for mass flow rate (Eq. (14)) and three for the power consumption (Eq. (13)).

Calorimeter data available from the manufacturer catalogue for 33 crankshaft compressors, 26 single-speed and 7 variable-speed with strokes spanning from 2 to 20 cm³, all running with HFC-134a, were used to verify the prediction capabilities of Eqs. (13) and (14) within and outside the range of the dataset, where the evaporating temperatures range from −35 °C to −10 °C, and condensing temperatures from 35 °C to 65 °C. During the fitting process, some coefficients reached values that minimized the error locally, but had no physical consistency, for instance $b_0 \equiv V_{sw} < 0$. To avoid such an issue, the coefficients were held constrained during the error minimization exercise, so that $a_{0..2}$, $b_{0..2} > 0$.

Furthermore, it is noteworthy that the results presented hereafter, in Sections 3.1 and 3.2, were achieved by using the entire dataset. In Section 3.3, however, there is a distinction between training and validation data, in order to evaluate the model performance regarding extrapolation or lack of data.

3.1. Single-speed compressors results

Fig. 4 shows the results obtained for the single-speed compressors, where 98% of the data points presented errors within ±10% for the mass flow rate, whereas for the power consumption approximately 93% of the data fell within the same bounds. No errors out of the ±20% thresholds were observed. Furthermore, it can be noticed in Fig. 4 that higher compressor displacements lead to better model performance. Samples of the fitting coefficients are summarized in Table 1, where a wide stroke span can be observed.

An additional capability of the model is the estimation of the compressor stroke from calorimetric data, obtained by multiplying the value of coefficient b_0 by R, the refrigerant gas constant. At all, the stroke of the 26 single-speed compressors were predicted with

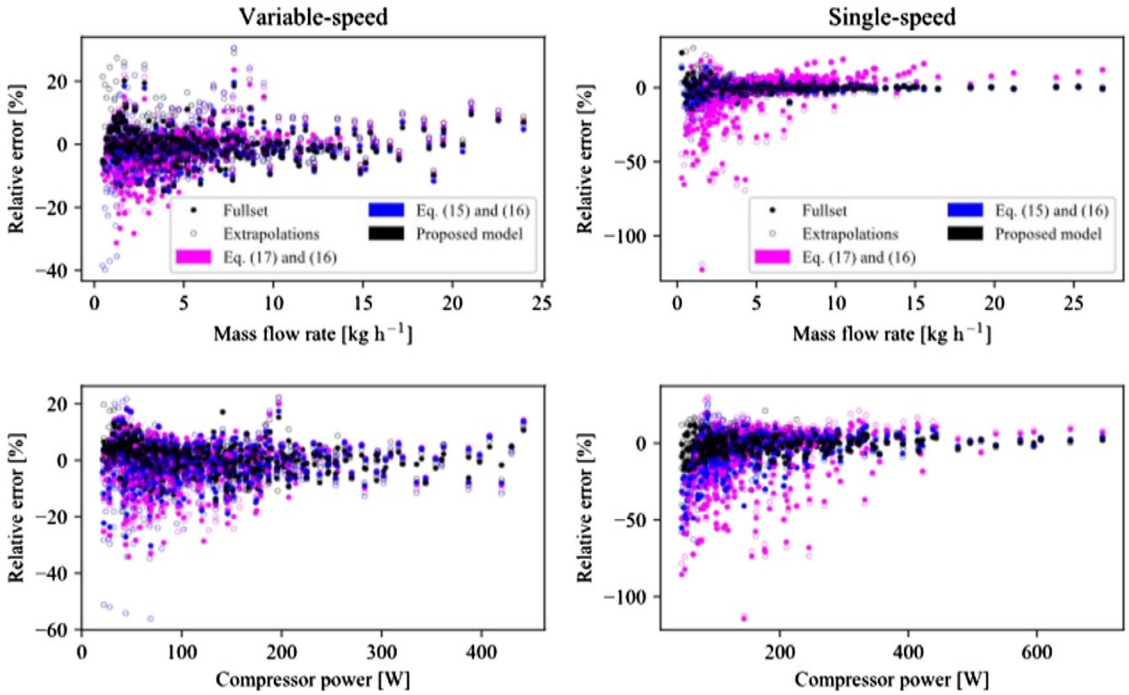

Fig. 9. Relative error of mass flow rate and compressor power when using less fitting coefficients.

Table 1
Fitting coefficients for some single-speed compressors at 60 Hz.

Nominal Stroke [cm^3]	a_0 / $b_0[\times 10^6]$[a]	a_1 / $b_1[\times 10^6]$[a]	$a_2[\times 10^{-3}]$ / b_2
2.83	29.495 2.72	0.999 0.204	47.3 0.686
3.40	57.696 3.23	0.792 0.223	39.4 0.635
4.60	36.669 4.59	0.892 0.84	46.6 0.44
5.54	32.388 5.26	0.87 0.392	45.6 0.639
6.36	31.519 6.63	0.874 1.545	42.2 0.399
7.95	26.222 7.42	0.854 0.07	40.1 1.213
9.26	51.576 8.23	0.78 1.397	50.5 0.392
12.11	65.609 10.52	0.701 3.392	53 0.254
20.44	110.581 17.7	0.573 1.253	34.7 0.706

[a] Multiplied by R (81.49 J kg^{-1} K^{-1}).

Table 2
Fitting coefficients for some variable-speed compressors.

Nominal Stroke [cm^3]	a_0 / $b_0[\times 10^6]$[a]	a_1 / $b_1[\times 10^6]$[a]	$a_2[\times 10^{-3}]$ / b_2
3.00	13.443 3.05	1.244 0.229	43.9 0.733
5.72	107.836 5.45	0.516 1.740	28.3 0.261
8.03	64.454 7.97	0.631 0.616	28.1 0.608
10.61	74.422 11.75	0.608 6.027	30.7 0.224

[a] Multiplied by R (81.49 J kg^{-1} K^{-1}).

an average RMS error of 7% and maximum deviation of 14%. In this case, since the speed N is fixed, it could be embedded into coefficients b_0 and b_1. However, it was kept out so that the compressor stroke can be compared straightforwardly with coefficient b_0.

3.2. Variable-speed compressors results

Variable-speed crankshaft compressors use an inverter to control the compressors speed N, therefore modulating the cooling capacity by changing the mass flow rate. In total, 7 different variable-speed compressors datasets with strokes ranging from 3 to 11 cm^3 and speeds spanning from 1200 to 4500 rpm were used to explore the model capabilities. The errors achieved for mass flow rate and compressor power are shown in Fig. 5, whereas the fitting coefficients can be seen in Table 2 for some samples of variable-speed compressors under analysis. As illustrated in Fig. 5, more than 95% of the experimental data agrees with the model predictions with errors below the ±10% thresholds for both mass flow rate and power consumption.

3.3. Extrapolation and data reduction

To further test the model capabilities, all coefficients were fitted again but using two different datasets: (i) disregarding the outer envelope data (all points with highest *or* lowest evaporating / condensing temperatures – and speed if applicable) and (ii) considering only the extreme data points (highest *and* lowest evaporating / condensing temperatures only), as illustrated in Fig. 6. The total number of training points used for coefficient regression in cases (i) and (ii) varied according to the compressor type, whether or not it was a VCC (variable-capacity compressor). For single-speed, compressors both cases (i) and (ii) datasets were comprised of 4 points (see Fig. 6). For VCCs, case (i) datasets had 8 points and case (ii) 6 points (note that the speed is considered in the extrap-

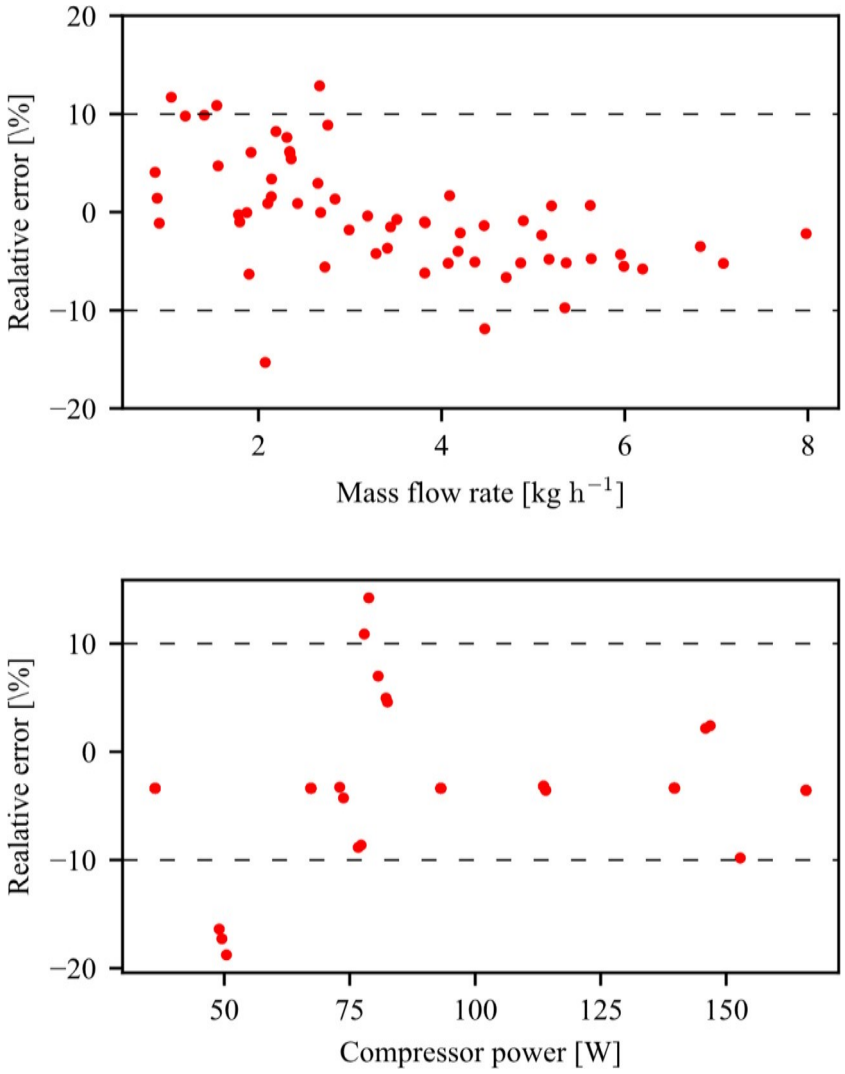

Fig. 10. Relative error of mass flow rate and compressor power for the oil-free linear compressor.

Table 3
Percentage of model predictions within $a \pm 10\%$ band, disregarding outer envelope (i) and considering only the extreme points (ii), as illustrated in Fig. 7.

	Single-speed		Variable-speed	
	$\dot{m}$	$\dot{W}$	$\dot{m}$	$\dot{W}$
Full set	97.4%	92.7%	95.1%	95.1%
Case (i)	90.0%	90.0%	94.8%	94.8%
Case (ii)	90.8%	90.8%	84.0%	84.0%

olation as well). Afterwards, the full dataset was used for the validation exercise, in such a way that data points that were not used for fitting the coefficients are used for error verification. Therefore, model extrapolations and dataset size can be evaluated by means of cases (i) and (ii), respectively.

Table 3 presents the percentage of the model predictions that showed errors within ±10%. To provide further evidence of the model robustness, Fig. 7 shows the error of fitting the model using case (i) and case (ii) datasets relative to using the full dataset. As one can see, case (ii) (i.e., using extreme data points only) lead to acceptable discrepancies, ranging from −10 to 5%, whereas the discrepancies observed for case (i) (i.e., extrapolations) spanned from −5 to 10%. Therefore, when extrapolating the range or using restrained datasets, the model deviates no more than ±10%.

Fig. 8 compares the prediction errors for variable-speed compressors obtained from the model proposed here and the one by Li (2012, 2013) in the cases where the entire dataset and a reduced dataset (case i) are available. As it can be seen in Fig. 8, the proposed model and Li (2013) model lead to similar results when the entire dataset is used – Li (2013) giving slightly better results. When the data is limited to cases (i) and (ii), the quadratic polynomials used by Li (2013) to fit the variable-speed efficiencies seem to introduce a non-physical trend which leads to large errors when either extrapolations take place or a reduced dataset was used.

3.4. Using less than three coefficients

The proposed model, in summary, is based upon Eqs. (8) and (12), and key selected parameters to be fitted from experimental data. Nonetheless, one could argue that fewer parameters could have been selected as the isentropic exponent (k) and the gas constant (R) are thermodynamic properties that can be easily obtained. Therefore, one coefficient might be dropped out so the model is as follows:

$$\dot{m} = \frac{p_s N}{R T_s}\left\{b_0 - b_1\left[\left(\frac{p_d}{p_s}\right)^{\frac{1}{k}} - 1\right]\right\} \tag{15}$$

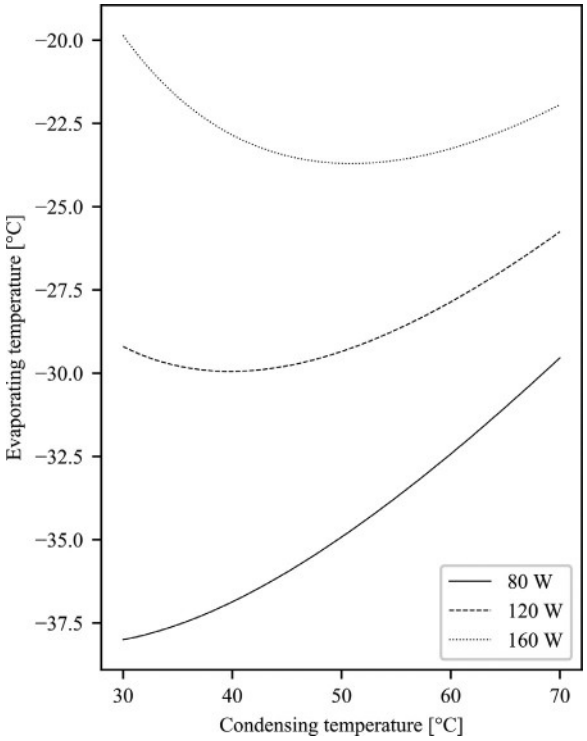

Fig. 11. Linear compressor operating thresholds.

$$\dot{W} = \dot{m}\left\{\frac{T_s}{a_0}\frac{Rk}{k-1}\left[\left(\frac{p_d}{p_s}\right)^{1-\frac{1}{k}} - 1\right] + a_1\right\} \tag{16}$$

Moreover, the swept volume can also be obtained from catalogue data, allowing the use of only one coefficient for the sake of mass flow rate calculations:

$$\dot{m} = \frac{p_s V_{sw} N}{R T_s}\left\{1 - b_0\left[\left(\frac{p_d}{p_s}\right)^{\frac{1}{k}} - 1\right]\right\} \tag{17}$$

Fig. 9 shows a comparison between the proposed model as is (Eqs. (13) and (14)), the proposed model dropping the coefficient that replaces $1/k$ (Eqs. (15) and (16)) and, the proposed model with the least possible number of fitting coefficients (Eqs. (17) and (16)). It can be seen from Fig. 9 that computing k as thermodynamic property slightly jeopardizes the model accuracy as the compression process taking place inside the cylinder is not isentropic. Also, it could be argued that the isentropic exponent, for ideal gases, is a function of temperature only, and experiences slight variations (1.14 at −70 °C and 1.1 at 70 °C for R134a) so that the assumption that it can be considered constant is in agreement with theory. Additionally, the use of the mass flow rate expression with a single coefficient, as in Eq. (17), depletes the model accuracy significantly, particularly for small capacity single-speed compressors, where the effects of clearance and the piston-cylinder leakage are far more expressive. Nonetheless, as there are so little degrees of freedom, extrapolations errors are not expressive – data points from extrapolated model are close to the points where the entire data set was used.

4. Variable-displacement linear compressor applications

Recognizing that a variable-displacement oil-free linear compressor is a variable-capacity reciprocating compressor which has the cooling capacity modulated through displacement in place of speed, thus Eqs. (13) and (14) should be also applicable to such an architecture. Noticing that the control signal of the compressor is the compression power $\dot{W}_{sig}$, so that the compressor uses the displacement needed to draw the power demanded, the mass flow rate can be calculated as a function of the compressor power. Therefore, isolating $\dot{m}$ in Eq. (13), the following expression for the mass flow rate can be obtained:

$$\dot{m}_{var} = \frac{\dot{W}_{sig}}{a_0 + a_1 T_s\left[\left(\frac{p_d}{p_s}\right)^{a_2} - 1\right]} \tag{18}$$

However, Eq. (18) does not take into account the geometric parameters of the compression cylinder, i.e., top and bottom dead centres. Therefore, in the cases where the power signal is higher than the power consumed by the compressor for the maximum stroke, i.e. when the piston reaches the top dead centre (see Fig. 1), the compressor operates at maximum displacement (fixed), a condition referred to hereafter as saturated displacement. When this occurs, the mass flow rate reaches its limiting value ($\dot{m}_{sat}$), becoming a function of the boundary conditions p_c, p_e and T_s only, as described by Eq. (14). Similarly, the power consumption at saturated displacement condition can be calculated from Eq. (13), as follows

$$\dot{W}_{sat} = \dot{m}_{sat}\left\{a_0 T_s\left[\left(\frac{p_c}{p_e}\right)^{a_1} - 1\right] + a_2\right\} \tag{19}$$

where the coefficients $a_{0..2}$ of Eqs. (18) and (19) are the same.

In summary, the application of the proposed model to variable-displacement linear compressors can be described as follows:

$$\dot{m} = \dot{m}_{var} \text{ and } \dot{W} = \dot{W}_{sig} \text{ if } \dot{m}_{var} < \dot{m}_{sat} \tag{20.a}$$

$$\dot{m} = \dot{m}_{sat} \text{ and } \dot{W} = \dot{W}_{sat} \text{ if } \dot{m}_{var} \geq \dot{m}_{sat} \tag{20.b}$$

The proposed model was used to fit the coefficients $a_{0..2}$ and $b_{0..2}$ for an oil-free linear compressor, based on proprietary experimental data provided by the manufacturer, where evaporating temperatures of −35, −25, −15 and −5 °C were used as well as condensing temperatures of 35, 45, and 65 °C (R134a) and power signals of 35, 65, 90, 110, 135 and 160 W (the compressor speed is mostly constant at around 120 Hz varying little in some operating conditions) totalizing 61 data points. Fig. 10 compares the model predictions with the experimental counterparts, where the entire dataset was used for fitting. About 87% of the mass flow rate data points were within the 10% error band, while 89% of the power consumption data fell in the same band. All data points were predicted with errors less than 20%. Furthermore, one should note that it appears as there are missing points on the compressor power chart in Fig. 10. Indeed, there are several overlapping points, which happens because the compressor is able to draw the power signal exactly, operating under a variable-displacement condition.

Finally, whether the linear compressor operates under saturated displacement or variable-displacement can be determined by combining Eqs. (14) and (19) to calculate the working temperatures, T_c and T_e, that saturate the displacement for a given power input. Fig. 10 shows the operating threshold, where the regions below the lines indicate that the compressor runs under saturated displacement. For instance, if the compressor shall operate at 40 °C and −30 °C of condensing and evaporating temperatures, respectively, a power input as high as 120 W could be used, as higher power signals would have no effect since the displacement is saturated.

5. Concluding remarks

A semi-empirical model for the vapour compression process was developed based on the fundamental theory of reciprocating compressors. The proposed model uses only three fitting coefficients for each performance indicator (power consumption and

mass flow rate), thus requiring a minimal dataset comprised of 3 datapoints, albeit in this study the smallest dataset used for model fittings was comprised of 4 datapoints (for single-speed compressors) and 6 datapoints (for variable-speed ones). An extended validation exercise was carried out, where extrapolation capabilities, and dataset sensitivity were verified against experimental data for single-speed, variable-speed, and linear variable-displacement reciprocating compressors. A total of 33 crankshaft compressors were used for validation purposes, being 26 single-speed and 7 variable-speed, with strokes ranging from 2 to 20 cm^3. For conventional single-speed compressors, approximately 97% of the mass flow rate and 93% of the power consumption data presented errors within the 10% thresholds. For variable-speed compressors, more than 95% of the datapoints presented absolute errors lower than 10% for both power consumption and mass flow rate.

A comparison between the presented model and the one devised by Li (2013) showed that, for full datasets, both display similar errors, whilst for restrained datasets the presented model performed much more robustly, with maximum errors by 27% as opposed to the 75% that Li (2013) has showed. Furthermore, the model was applied to a variable-displacement oil-free linear compressor, where more than 85% of the model predictions fell within the 10% error thresholds, for both mass flow rate and compression power. In addition, it was possible to put forward an operation map for said compressor, where saturation lines show the evaporation/condensing temperatures where the compressor is able to modulate its capacity. Due to the semi-empirical nature of the model, and as a complementary perk, it was possible to estimate the compressors stroke through the fitted coefficients, where an average 7% RMS error was observed and maximum deviation of 14% for all compressors under analysis. The usage of purely mathematical functions to fit physical data, as in Li's (2013) model, may bring about non-physical trends that are likely to show up in extrapolation exercises, particularly with polynomials fitted using small data sets, which can show strong curvatures.

Acknowledgements

This study was performed under the auspices of the Brazilian Government funding agencies CAPES, CNPq and Embrapii. The continuous support from the company Embraco is also duly acknowledged. The authors are also thankful to Mr. Fabian Fagotti (Embraco), who kindly reviewed the manuscript.

References

ASHRAE Standard S23, 1993. Methods of Testing for Rating Positive Displacement Refrigerant Compressor and Condensing Units. American Society of Heating, Refrigeration and Air Conditioning Engineers, Atlanta, GA, USA.

Cheung, H., Wang, S., 2018. A comparison of the effect of empirical and physical modeling approaches to extrapolation capability of compressor models by uncertainty analysis. A case study with common semi-empirical compressor mass flow rate models. Int. J. Refrig. 86, 331–343.

Choi, S., Han, U., Cho, H., Lee, H., 2018. Review: recent advances in household refrigerator cycle technologies. App. Therm. Eng. 132, 560–574.

Diniz, M.C., Melo, C., Deschamps, C.J., 2018. Experimental performance assessment of a hermetic reciprocating compressor operating in a household refrigerator under on–off cycling conditions. Int. J. Refrig. 88, 587–598.

Gosney, W.B., 1982. Principles of Refrigeration. Cambridge University Press, Cambridge: New York.

Haberschill, P., Borg, S., Mondot, M., 1994. Hermetic compressor models determination of parameters from a minimum number of tests. In: Lallemand, M. (Ed.), Proceedings of the International Compressor Engineering Conference at Purdue. West Lafayette, IN, USA Paper 969.

Hermes, C.J.L., Melo, C., 2006. How to get the most out from a semi-empirical reciprocating compressor using a minimum set of data. In: Proceedings of the 6th International Conference on Compressors and Coolants. Slovak Republic September 27-29, Casta Papiernicka.

Hermes, C.J.L., Melo, C., 2008. A first-principles simulation model for the start-up and cycling transients of household refrigerators. Int. J. Refrig. 31, 1622–1630.

Hu, J., Yang, L., Shao, L.-.L., Zhang, C.-.L., 2014. Generic network modeling of reciprocating compressors. Int. J. Refrig. 45, 107–119.

Jahnig, D.I., Reindl, D.T., Klein, S.A., 2000. Characterization of refrigeration system compressor performance. ASHRAE Trans. 106 (2), 122–130.

Lee, S., Singh, R., Moran, M.J., 1982. First Law Analysis of a Compressor Using a Computer Simulation Model. In: Proceedings of the International Compressor Engineering Conference, West Lafayette-IN, USA, Paper 396.

Li, W., 2012. Simplified steady-state modeling for hermetic compressors with focus on extrapolation. Int. J. Refrig. 35, 1722–1733.

Li, W., 2013. Simplified steady-state modeling for variable speed compressors. App. Therm. Eng. 50, 318–326.

Liang, K., 2017. A review of linear compressors for refrigeration. Int. J. Refrig. 84, 253–273.

Mackensen, A., Klein, S.A., Reindl, D.T., 2002. Characterization of refrigeration system compressor performance. In: Proceedings of the International Refrigeration Conference at Purdue West Lafayette- IN, USA Paper R9-1.

Navarro, E., Granyrd, E., Urchueguía, J.F., Corberán, J.M., 2007. A phenomenological model for analyzing reciprocating compressors. Int. J. Refrig. 30, 237–242.

Negrão, C.O.R., Erthal, R.H., Andrade, D.E.V., Silva, L.W.da, 2011. A semi-empirical model for the unsteady-state simulation of reciprocating compressors for household refrigeration applications. App. Therm. Eng. 31 (6), 1114–1124.

Oliveira, V.de, Trofino, A., Hermes, C.J.L., 2011. A switching control strategy for vapor compression refrigeration systems. App. Therm. Eng. 31, 3914–3921.

Piedrahita-Velásquez, C.A., Ciro-Velásquez, H.J., Gómez-Botero, M.A., 2014. Identification and digital control of a household refrigeration system with a variable speed compressor. Int. J. Refrig. 48, 178–187.

Popovic, P., Shapiro, H., 1995. A semi-empirical method for modeling a reciprocating compressor in refrigeration systems. ASHRAE Trans. 101, 367–382.

Prata, A. T., .Ferreira, R. T. S., Fagotti, F., & Todescat, M. L. (.1994). Heat transfer in a reciprocating compressor., IN, USA: West Lafayette.

Roskosch, D., Venzik, V., Atakan, B., 2017. Thermodynamic model for reciprocating compressors with the focus on fluid dependent efficiencies. Int. J. Refrig. 84, 104–116.

Stouffs, P., Tazerout, M., Wauters, P., 2001. Thermodynamic analysis of reciprocating compressors. Int. J. The. Sci. 40, 52–66.

Tuhovcak, J., Hejcik, J., Jicha, M., 2016. Comparison of heat transfer models for reciprocating compressor. App. Therm. Eng. 103, 607–615.

Yang, M., Jung, C.W., Kang, Y.T., 2015. Development of high efficiency cycles for domestic refrigerator-freezer application. Energy 93, 2258–2266.